Flexible and Printed Electronics

Flexible, scalable, and efficient thermoelectric touch detector based on PDMS and graphite flakes

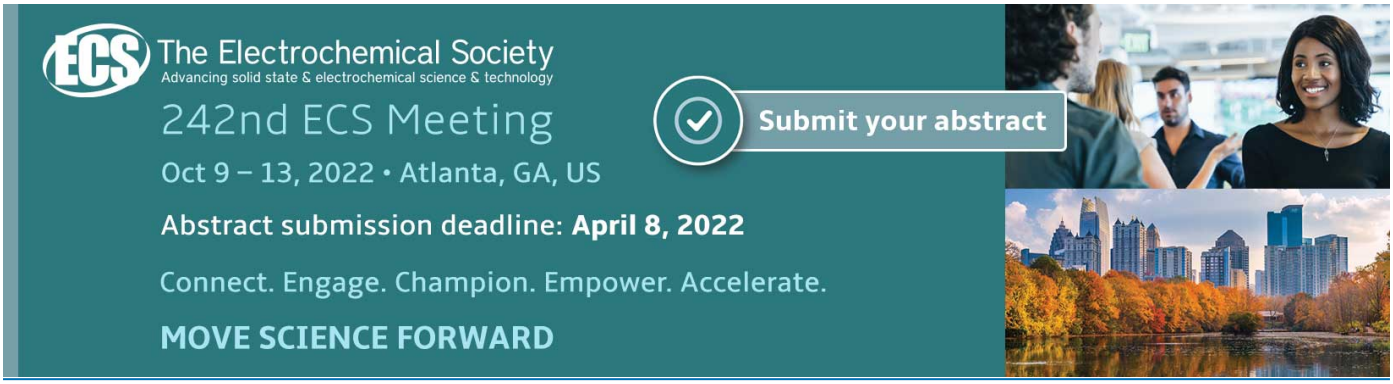

IOP Publishing Flex. Print. Electron. 6 (2021) 045018 https://doi.org/10.1088/2058-8585/ac45de

Flexible and Printed Electronics

OPEN ACCESS

RECEIVED
19 October 2021

REVISED
2 December 2021

ACCEPTED FOR PUBLICATION
22 December 2021

PUBLISHED
6 January 2022

PAPER

Flexible, scalable, and efficient thermoelectric touch detector based on PDMS and graphite flakes

Joana Figueira[1], Joana Loureiro[1], Eliana Vieira[2], Elvira Fortunato[1], Rodrigo Martins[1] and Luís Pereira[1,*]

[1] i3N/CENIMAT, Department of Materials Science, NOVA School of Science and Technology, Universidade NOVA de Lisboa and CEMOP/UNINOVA, Campus de Caparica, 2829-516 Caparica, Portugal
[2] CMEMS-UMINHO, University of Minho, Campus Azurem, 4804-533 Guimaraes, Portugal
[*] Author to whom any correspondence should be addressed.

E-mail: lmnp@fct.unl.pt

Keywords: thermoelectric touch sensors, PDMS/graphite flakes, flexible technologies, no substrates, low-cost fabrication, scalable manufacturing

Abstract

This paper presents freestanding thermoelectric touch detectors consisting of graphite conductive flakes into a polydimethylsiloxane matrix. An optimal concentration of graphite flakes (45 wt%) lead to robust and homogeneous detectors that exhibited signal-noise ratio values up to 170 with rise and falling times below 1 s and 7 s, respectively. The detectors performance was stable over continuous operation and did not reveal significant degradation while bended under different curvature radii (45, 25 and 15 mm) and consecutive bending cycles. Moreover, the twist of the thermal gradient direction between the electrodes of the detector enables a Yes or No response which opens new usage possibilities. Therefore, this work provides an efficient way to develop robust, low-cost, and scalable thermal detectors with potential use in wearable technologies.

1. Introduction

Within the concept of the Internet of Things there is an emerging class of devices that are worn in, on and around the human body and are able to sense, record and exchange data with surrounding networks. Nowadays, temperature sensing plays a pivotal role in a range of healthcare monitoring applications. Furthermore, body temperature can be used to detect human touch in combination with thermoelectric (TE) technology. Skin temperature can change from 25 °C to 36 °C at an ambient temperature range of 4 °C to 40 °C [1], giving rise to temperature gradients up to 21 °C, enough for sensing or detecting applications where organic materials can be used to obtain low-cost and scalable TE devices that work at room temperature. Such approach can provide an alternative to conventional capacitive sensing technologies.

When touched, a TE detector converts the thermal gradient generated between the skin and the detector into an electrical signal. Among several desirable features, this kind of device should have a high sensing performance (such as, high and stable signal-noise ratio (SNR) values with fast response), good mechanical properties and, not less meaningful, it should be low-cost and suitable for scalable manufacturing [2]. The TE touch performance is strongly correlated with the TE performance of the chosen materials. Particularly, large Seebeck coefficient values (S) translate directly into high signal levels (signal to noise ratio) for thermal sensing [3]. Moreover, high electrical conductivity (σ) reduces the Joule heating and increases the TE voltage generated [4]. Therefore, a high-power factor $PF = S^2.\sigma$ is essentially required. Electronically, a detector with a V_{signal}/V_{noise} ratio of at least 3:1 [5] or even 5:1 [6] is desirable to maintain a robust operation, where V_{signal} is the output voltage (above noise level) and the V_{noise} is the background noise (standard deviation of the signal during resting mode). Several researchers have reported SNR up to 35 for TE detectors, choosing different materials and techniques. Ruoho *et al* [3] reported a TE touch panel based on Al-doped ZnO active material with a SNR of 20, and a rise time of 90 ms. A similar SNR value was reported by Vieira *et al* [7] for 60 nm—SnO_x thin films with a fast fingertip touch event. The authors reported a SNR ≈10 for a 60 nm thick-Cu_2O

film [8]. Recently, Koskinen *et al* [9] presented a high SNR of 35 for a touch sensing device made by multilayer graphene ink. This SNR range enables the detection, without any doubt, of individual touches. However, most of these state-of-art results come from highly costing techniques (vacuum deposition systems or high temperature steps) and/or rigid substrates.

Poly-(dimethylsiloxane), commonly known as PDMS, is an elastomer widely used in several research areas, such as microfluidics or stretchable electronics, suitable either as substrate or as composite matrix material. PDMS is an environmentally friendly material, optically transparent, viscoelastic, chemically, and thermally stable, highly flexible, and hydrophobic. It requires low curing temperatures, can easily be molded with high resolution and aspect ratio [10–12], and can have its viscosity manipulated [13]. There are several reports about PDMS composites where the PDMS properties were modified and optimized by adding other materials: composites with Ag micro sized flakes and carbon black [10, 14] for flexible electronics without the need of metallization, ZnO and CuO nano particles [15, 16] to form coatings with anticorrosion and antifouling properties, PZT micro particles [17] for piezoelectric devices, boron nitride [18] for wearable pressure sensing systems, graphite flakes [11, 12] for flexible temperature sensors, and graphene nanoplatelets [19] for photoresponsive actuations.

Graphite is known to have a TE response when thermally stimulated and it is much cheaper when compared to carbon nanotubes and graphene [20], which are some of the reasons explaining the researchers' interest in this material. Several reports were published using graphite in the TE area [20–22] and also on strain and temperature sensors [12, 23] but as far as we know there are no published work with thermoelectric sensors based on PDMS and graphite composites.

In this work, we report a flexible TE device for human touch detection, using graphite flakes into a PDMS matrix as the functional sensor material. The device enables a *Yes* or *No* response depending on the touched pad. Different composites were developed by changing the graphite flakes weight concentration (40, 45 and 50 wt%). The TE performance was evaluated, and the results correlated with the morphological results. Moreover, the touch detector properties were investigated for the 45 wt% G_{Flakes} composite, the one with optimized properties.

Moreover, this sensor offers a good performance both for naked finger and covered finger as the thermal gradient is still present between the finger and the detector. This feature is important, namely in industrial processes, patient-care activities, laboratory safety, among others, especially in a pandemic situation like the one we are living.

2. Results and discussion

The ability to originate a smooth surface drastically decreases when going from 40 up to 50 wt% G_{Flakes}, because the viscosity of the PDMS mixture increases with the G_{Flakes} weight content, as can be seen from the SEM images of figures 1(a)–(c). In terms of processability, it is much easier to mix and to cast mixtures up to 45 wt%, leading to more robust and homogeneous samples. For mixtures with 50 wt%, the cohesion limits are being surpassed. In fact, mixtures up to 45 wt% enabled the use of the film casting technique, with an adjustable micrometer film applicator moved by an automatic arm. With this method, films with thickness down to 0.2 mm were obtained for the 40 wt% G_{Flakes}. For the 50 wt% mixture, a blade coating technique had to be used instead of the film casting one because the film was breaking apart while being casted.

Hall effect measurements were carried out on samples with different G_{Flakes} wt% and the main results are depicted in figure 1(d). When the G_{Flakes} wt% increased from 40 to 50 wt% the mobility of the majority carriers decreased from 2.7 to 0.1 $cm^2\,(V.s)^{-1}$ (orange triangles) while their concentration increased from 1016 to 1019 cm^{-3}. Increasing the G_{Flakes} wt% in a composite results in a loss of the polymer content, which significantly enhances the carriers' concentration of the material and at the same time reduces their mobility (even with fewer interfaces between the two different materials). Although this so-called trade off is happening, since the collisions between carriers increase with the carrier concentration [24], there is an electrical conductivity improvement by almost two orders of magnitude (green stars).

As expected, and presented in figure 1(e), the S is positive (blue circles), indicating a p-type material (meaning the majority carriers are holes) and it slightly decreases as the G_{Flakes} wt% increases. These S values are in accordance with previous published results 23 where a similar value ($+18\ \mu V\ K^{-1}$) was described for bulk graphite samples. The slightly S decrement from 18 $\mu V\ K^{-1}$ to 14 $\mu V\ K^{-1}$ [25] alongside with the σ increment is once again a well-known trade off due to the existence of more carriers [26, 27]. Evaluating these graphite percentage-dependent properties we conclude that there is a Power Factor, PF, enhancement (purple triangles), from 0.19 to 3.8 nW $(m.K^2)^{-1}$ for G_{Flakes} wt% from 40 to 50, respectively. Beside these interesting TE results, it is important to emphasize that this composite is low-cost, environmentally friendly, is flexible, available, biocompatible and benefits of easy processing. Furthermore, this composite can be used to build TE elements that do not need any substrate, therefore minimizing the thermal contact resistance between the electrical device and the heat sink [26].

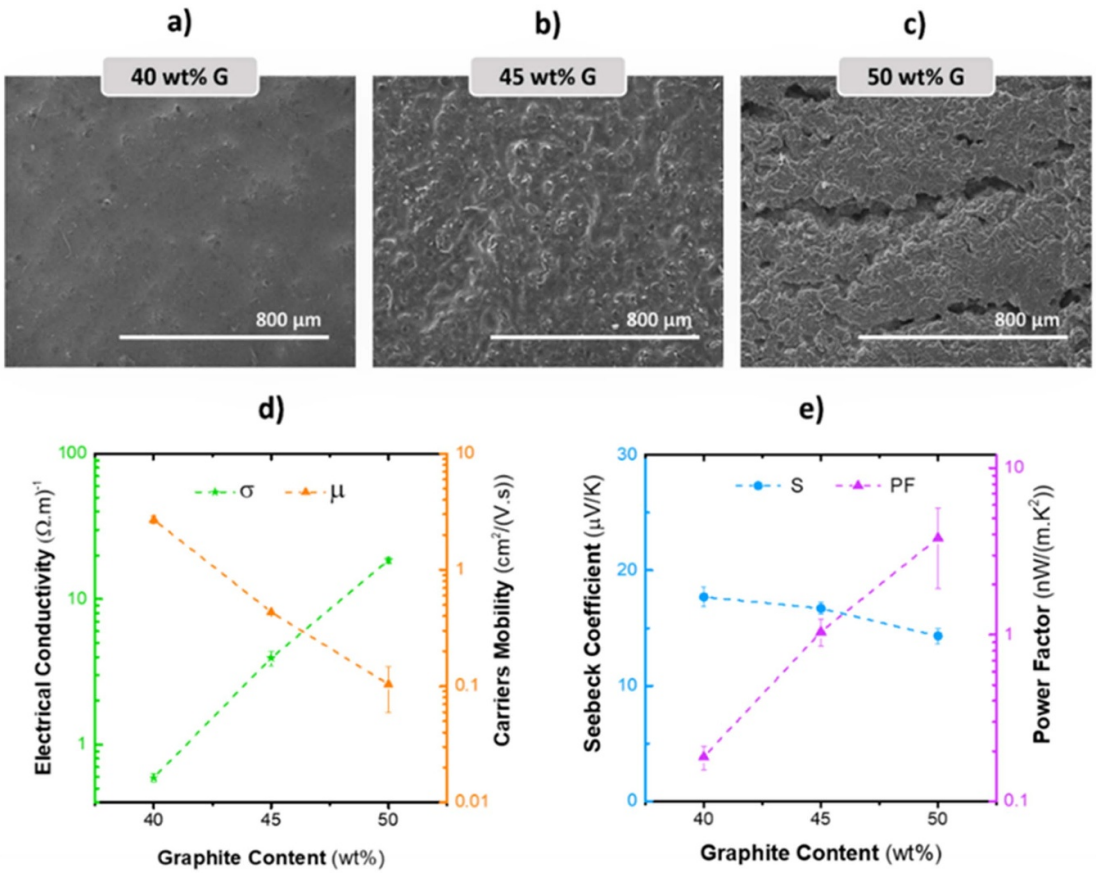

Figure 1. Surface SEM images of PDMS: GFlakes samples with different wt% GFlakes (a) 40 wt% GFlakes; (b) 45 wt% GFlakes and (c) 50 wt% GFlakes. Graphics of (d) Electrical conductivity and carriers' mobility, obtained through Hall Effect measurement, and (e) Seebeck coefficient (S) and Power Factor (PF) vs wt% GFlakes. Error bars are also shown.

Human touch detection was chosen as the proof-of-concept application for the developed composites. In figure 2, the open circuit voltage is depicted showing the effect of touching (1–2 s of thermal contact) on one of the electrodes, V_{ON}. Briefly after the event, the signal returns to the initial state, V_{OFF}. The touch response was the same despite the wt% G_{Flakes}. V_{ON} is the response to the temperature rise caused by the finger touch and has no relation to skin interaction since similar results were obtained with the finger covered. In figure 2, the SNR value is presented for each touching peak, which evaluates the amplitude of the signal against the noise. The SNR was calculated by $(V_{ON}–V_{OFF}\_mean)/stdev\_V_{OFF}$ [5], and we can see that the maximum of 130.4 is achieved for the 45 wt% G_{Flakes} device (green curve). The 50 wt% device is the one with the lowest SNR and this composite presented the highest PF, but the lowest S of the three being tested. Although the 50 wt% composite has shown the best PF, it also shows the lowest S value, which is more important than σ when referring to this type of application. In terms of thermal conductivity, the higher the composite k, the higher the risk of having interferences in the thermal gradient created by the finger touch. Based on literature [28], we can predict that k increases with the amount of G_{Flakes} added to the PDMS. The PDMS k is around 0.2 W (m.K)$^{-1}$ [12, 29], while for bulk graphite flakes a $k \sim 1.4$ W m.k^{-1} was reported [29]. This said, and because SEM images also show that the 45 wt% G_{Flakes} samples are more homogeneous and without visible cracks, this was the chosen composition to perform other touching tests.

A device with 45 wt% G_{Flakes} was characterized in different bending configurations to check the possibility to be used in applications where bending is relevant. In the first test the device was measured while bended with three different curvature radii (figure 3(a)). Figure 3(b) shows the device voltage response to touch while being bended, starting with the largest curvature radius, 45 mm (blue curve), passing to 25 mm (orange curve) and ending with the smallest curvature radius, 15 mm (purple curve). The results show that the behavior of the device is not affected by the curvature radii, neither in terms of time response nor in the SNR value (showing only a slight decrease of 10% when the curvature radius decreased down to 15 mm).

A long static test was performed with the device being characterized over 40 h while fixed on a surface

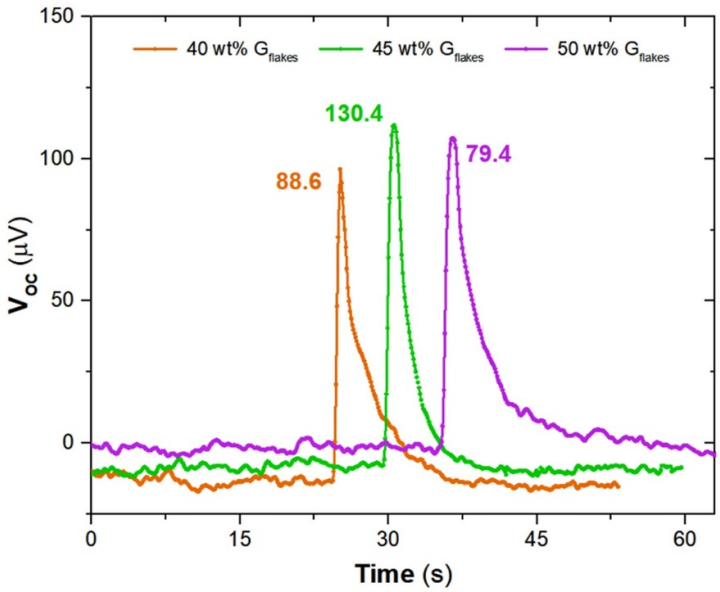

Figure 2. Voltage response (V_{OC}) of the PDMS: G_{Flakes} devices to finger touch events. Each color corresponds to different G_{Flakes} wt%. Signal-to-noise ratio values are depicted for each touching peak. The difference in time between the signal peaks is promoted for better visualization.

with a curvature radius of 15 mm. Figure 3(c) shows de results immediately after the bending step (light green curve), 20 h after it (yellow curve) and finally 40 h after (orange curve). We can observe that even when bended with a 15 mm curvature radius during 40 h, continuously, the device behavior keeps similar to the planar measurement one, both in terms of time response and SNR values. The only characteristic that slightly changed is the V_{OFF}, which is correlated to an increase of the device resistance due to the bending stress (which triplicated when comparing the starting time point with the 40 h time point), although it does not affect the device SNR.

Regarding dynamic stress evaluation (figure 3(d)), the test started with the device being characterized in a flat mode (black curve), then it was submitted to 30 bending cycles with 25 mm curvature radius and, once again, characterized in a flat mode (dark green curve). Afterwards, the same sequence was repeated completing 60 cycles in total (light green curve). As in the two previous bending tests, it can be observed that the device behavior is not affected by the dynamic bending test (the SNR and time responses kept constant over the cycling).

The bending tests performed and depicted in figure 3 also show that the V_{ON} value is larger when the device is measured over the curved surface rather than measured in a flat mode. This is most probably explained by the type of surface where the device is characterized rather than any explanation associated with the curvature itself. The cylinders used for the bending tests are metallic which means they act as dissipators and contribute to an increase of the thermal gradient arising from the finger touch, consequently increasing the V_{ON}.

2.1. Yes or No response application

When a TE material is subjected to a thermal gradient, the majority carriers move from the hot to the cold side which means that when we have a p-type material the holes flow from the hot to the cold side and electrons go the other way around. If the thermal gradient direction is inverted, carriers will also invert their path, which will originate a symmetric electrical response (if the measurement system remains unchanged).

The distance between contacts has influence in the thermal gradient since it affects the time needed to reach a thermal equilibrium between sites. Decreasing the contacts distance means decreasing the thermal gradient and, consequently, the V_{ON} value. The area of the electrodes, which is the area available for heat collection, also interferes with the V_{ON} value. Larger metallic pads can collect heat more efficiently than smaller ones (as the finger touch area increases). This said, electrodes design plays an important role in the device performance, and they can be optimized for higher and faster SNR values or even manipulated to have asymmetric positive/negative peaks.

In figure 4(a), there is a scheme of the quick *Yes* or *No* response test, showing the results from a sample tested in a flat mode (figure 4(b)) and also bended with a 15 mm curvature radius (figure 4(c)). Beside the previously explained differences in the V_{ON} (due to the metallic surface of the cylinder) the performance of the device is the same in the two situations, with SNR always above 100, proving again that it can be used both in flat mode or bended (at least down to a 15 mm curvature radius).

The response time of the touch detectors, which is reflected in the rise (τ_{rise}) and fall (τ_{fall}) times,

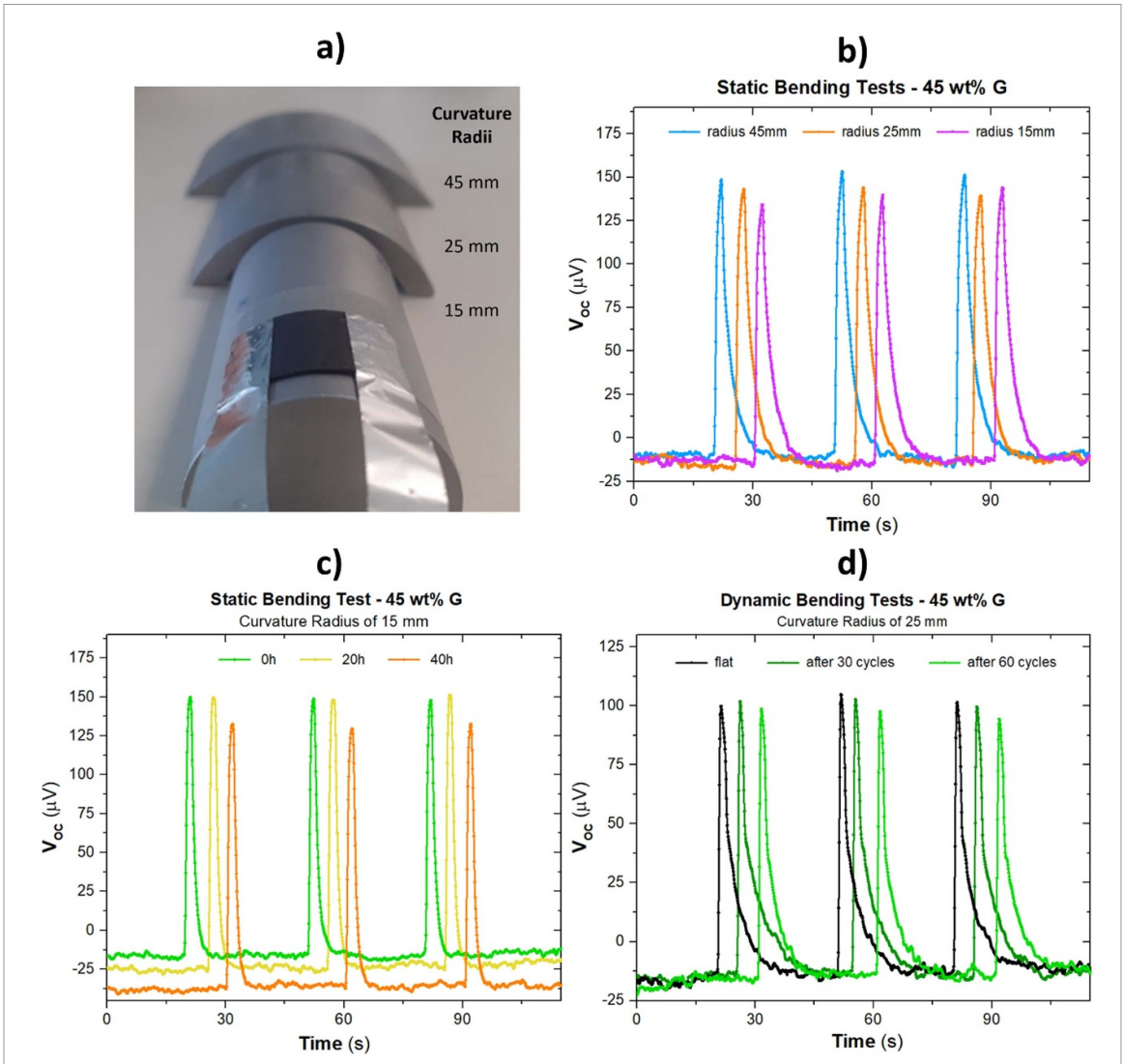

Figure 3. (a) Metallic cylinders with different curvature radii, 45, 25 and 15 mm; (b) static bending test results using the three different metallic cylinders; (c) static bending tests on the 15 mm cylinder, over time and (d) dynamic bending tests using the 25 mm cylinder. The difference in time between the signal peaks is promoted for better visualization.

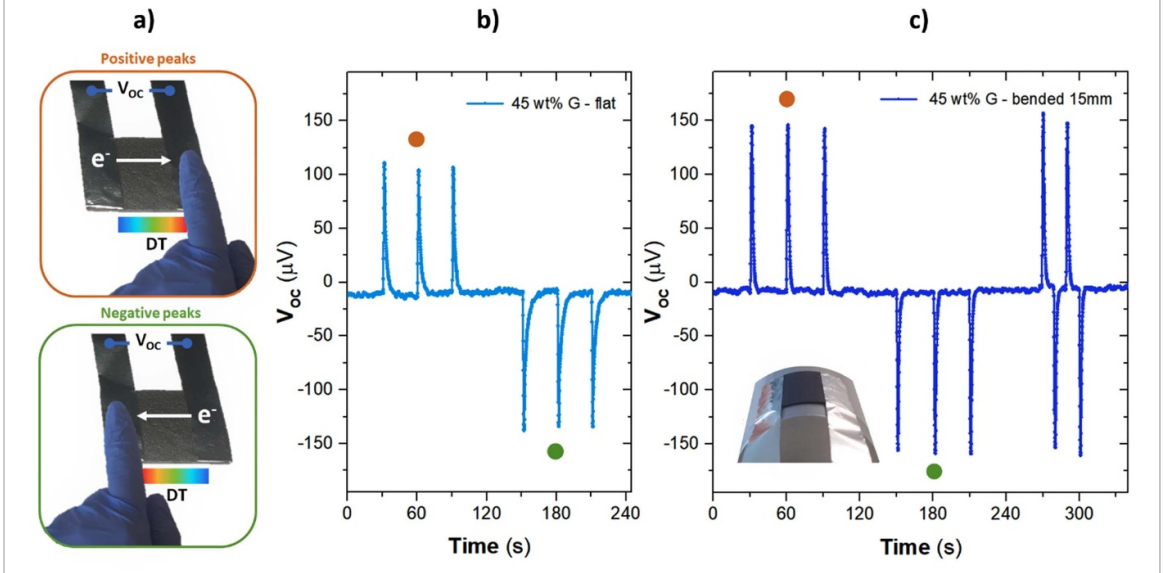

Figure 4. (a) Gloved finger touch scheme for a *Yes* and *No* response test based on symmetric thermal gradient; (b) V_{OC} electrical characterization in a flat configuration and (c) with a 15 mm curvature radius.

was calculated by normalizing the curves and measuring the time required for the V_{OC} to increase from 10% to 90%, and then to decrease from 90% to 10% of its maximum value. Results show fast rise times, always bellow 1 s for both configurations. Regarding the fall times, and because the thermal conductivity of the characterization supports is different, values bellow 7 s were observed for the flat mode, which has a lower *k*. Smaller values, below 3 s, were observed for the bended mode, which has a higher *k* that helps the thermal gradient $\sim 0\ K$ state recovery. These results mean that these devices can be used for fast/real-time human touch electrical trigger/detector using standard electronics (like Arduino) to read the output voltages.

3. Conclusion

The design, production, characterization, and optimization of touch detectors based on PDMS/G_{Flakes} composites are showcased in this work. The advantages of these devices lie in its simple and low-cost fabrication, and low temperature processes, achieving relevant and reproducible performances. Additionally, these devices do not require the support of an extra substrate. Moreover, the capacitive touch sensors need a conductive object to operate which eliminates many other touch objects, such as gloved finger.

Different wt% G_{flakes}—40, 45 and 50 wt%—were obtained through a simple fabrication method, and further characterized. All samples have major p-type electrical conductivity, being that with the increase of graphite it was observed an increase in the carrier concentration and consequent increase in the electrical conductivity and at the same time a decrease in the Seebeck coefficient value.

The touch detector performance based on the composite with 45 wt% G_{Flakes} was evaluated for a *Yes* or *No* application, in its flat and bended configurations, and revealed short rise and fall times, with SNR values between 100 and 170. These results are highly promising for fast real time human touch applications.

4. Experimental section

4.1. Materials

PDMS (184 Silicone Elastomer Base and 184 Silicone Elastomer Curing Agent) was purchased from SYLGARD™ and graphite flakes, GFlakes (mesh 325, 99.8%, metal basis) were purchased from Alfa Aesar®, and used as received. Commercial carbon screen paste (CRSN2644, from SunChemical®) and commercial aluminium foil (12 μm thick) were used to create the electrodes and conductive paths.

4.2. Samples and devices preparation

To prepare the PDMS, the elastomer base and the curing agent were mixed (in a 10:1 ratio) and taken to the exicator to remove the air bubbles formed during their reaction. Different amounts of graphite flakes (40, 45 and 50 wt%) were manually mixed till a homogeneous mixture is achieved. This mixture was once again put in the exicator although this time much less air bubbles can come out, since the viscosity in most cases is extremely high at this point. It was observed by our experiments that composites with wt% of G_{Flakes} higher than 50% becomes very difficult to dispense due to the high viscosity. Therefore, the composite tends to break, since the PDMS is no longer able to agglomerate the G_{Flakes}. On the other hand, below 40 wt% of G_{Flakes} the composites become high resistive ($\approx$ few MΩ), which turns impossible to connect several elements in series, for example. Furthermore, the PDMS is a material that expands when it is heated, and contracts when it is cooled. In this sense, when the PDMS content is higher than G_{Flakes}, the deformations on PDMS will break the connection between the flakes, leading to variations in the resistance of the composites, which is not desirable.

To achieve homogeneous thin films, the samples were obtained by blade coating or film casting the composite mixtures (depending on the amount of graphite flakes) and then cured at 70 °C in an oven, being the time dependent on the thickness of the samples (usually between 35 and 50 min). After the curing step, the material was detached from the support substrate (acetate sheet) and robust samples with thicknesses between $\approx$0.2 and $\approx$1.1 mm were obtained, without any need of substrate. Afterwards, these films were cut in the desired shape and the electrical connections between elements were done, using Carbon ink to glue the Al foil, having a drying/curing step of 30 min at 100 °C in a hot plate. The mixture and blade coating processes, as well as the desiccator and oven steps, were optimized to obtain homogeneous mats and cut samples, with reproducible results for the tested thicknesses.

A scheme of the described process can be seen in figure 5. The graphite supplier specifies that the morphology is flaked, and that the particles size is adequate for the 325-mesh used in screen printing process, which means that particles need to have a dimension bellow 44 μm in order to pass its openings. This information is confirmed by SEM image (figure 5, left side), where we observe G_{flakes} with a wide range of sizes but not exceeding $\approx$40 μm.

4.3. Samples characterization

The morphology of G_{Flakes} of the casted films was examined by scanning electron microscopy (SEM) using a Hitachi TM3030Plus tabletop workstation (Tokyo, Japan). The Seebeck coefficient (*S*) of PDMS: G_{Flakes} samples was measured at room temperature,

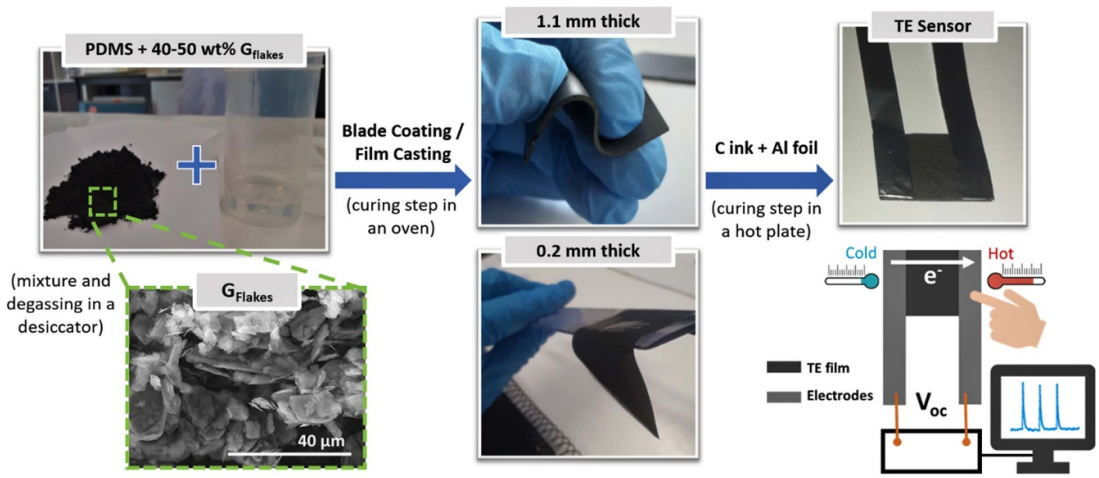

Figure 5. Fabrication scheme for producing the thermoelectric (TE) touch sensors based on PDMS: G_{Flakes}. The touch of the human finger leads to the creation of a temperature gradient in the TE film, and therefore an electromotive force is generated by moving a carrier inside the thermoelectric element. A representative scanning electron microscope (SEM) image of the used commercial G_{Flakes} is also shown.

in a planar configuration using a homemade setup based on the 'two-probe' method [7]. This method consists in connecting one side of the film to a heated metal block at a fixed temperature (the block is heated by the application of successive voltage values, between 1 and 3 V) using the DC programmable source (Yokogawa model 7651) and the other side to a heat sink at room temperature, to generate a few temperatures difference (ΔT) along the film. The ΔT was measured using platinum wire resistors, Pt-100 (100 Ω at 0 °C precision resistor) employed in the two metal blocks. The resulting thermovoltage (ΔV) is measured by Agilent 34 410 A 61/2 Digit Multimeter. A linear plot of ΔV versus ΔT is expected, which is representative of a good thermal contact between the film and the blocks. S values and corresponding errors are obtained using the LINEST function in EXCEL program. This function uses the least squares method to calculate the statistics for a straight line (that best fits the experimental data) and returns an array of parameters describing that line, including S (from the slope of the linear fitting), and error. The carrier Hall mobility, electrical conductivity and carrier concentration were measured with a Biorad/Nanometrics HL5500 Hall effect system, using van der Pauw contact geometry. The samples for Hall measurement were cut in quadrangular shapes and covered with C ink contacts at the corners.

4.4. Devices characterization

The thermoelectric responses of the samples were obtained using a Gamry Instruments Reference 600 Potentiostat in a configuration where the open circuit potential (V_{OC}) is measured over time, while touching (or not) the sample with the gloved finger.

Flexibility tests were done by touch detection characterization while resorting the device to static and dynamic bending stresses, using cylinders with curvature radii of 45, 25 and 15 mm. The effect of long period bending stress was also evaluated by fixing the device over the smallest curvature radius cylinder (15 mm) and characterizing the evolution of its touch detection performance and electrical properties over time.

Data availability statement

All data that support the findings of this study are included within the article (and any supplementary files).

Acknowledgments

This work was supported by the FEDER funds through the COMPETE 2020 Program and the National Funds through the FCT—Portuguese Foundation for Science and Technology under the Project No. POCI-01-0145-FEDER-007688, Reference UID/CTM/50025. J F thanks the support from FCT—Portuguese Foundation for Science and Technology through the PhD scholarship SFRH/BD/121679/2016 (Joana Figueira) and E V thanks the FCT national funds, under the national support to R&D units grant, through the reference project UIDB/04436/2020 and UIDP/04436/2020. The authors would like to acknowledge the European Commission under project NewFun (ERC-StG-2014, GA 640598) and Synergy (H2020-WIDESPREAD-2020-5, GA 952169), GA 692373). The authors would also like to acknowledge Jenny Boane for SEM images.

Conflict of interest

The authors declare no conflict of interest.

ORCID iDs

Joana Figueira https://orcid.org/0000-0002-5996-9831
Joana Loureiro https://orcid.org/0000-0001-9926-4898
Eliana Vieira https://orcid.org/0000-0001-8198-6024
Elvira Fortunato https://orcid.org/0000-0002-4202-7047
Rodrigo Martins https://orcid.org/0000-0002-1997-7669
Luís Pereira https://orcid.org/0000-0001-8281-8663

References

[1] Thielen M 2018 Thermal and electrical energy converters and interfaces for the internet of humans *PhD Thesis*
[2] Gong X, Zhang L, Huang Y, Wang S, Pan G and Li L 2020 *RSC Adv.* **10** 22222–9
[3] Ruoho M, Juntunen T, Alasaarela T, Pudas M and Tittonen I 2016 *Adv. Mater. Technol.* **1** 1600204
[4] Banik A, Perumal S and Biswas K 2019 Thermoelectric properties of metal chalcogenides nanosheets and nanofilms grown by chemical and physical routes *Thermoelectric Thin Films* (Cham: Springer) pp 157–84
[5] Bender L (Brun-Conti) 2013 *Encyclopedia of Forensic Sciences* (Cambridge, MA: Elsevier) pp 273–8
[6] Schmitz M, Khalilbeigi M, Balwierz M, Lissermann R, Mühlhaüser M and Steimle J 2015 *UIST 2015—Proc. 28th Annu. ACM Symp. User Interface Softw. Technol.* pp 253–8
[7] Vieira E M F, Silva J P B, Veltruská K, Matolin V, Pires A L, Pereira A M, Gomes M J M and Goncalves L M 2019 *Nanotechnology* **30** 435502
[8] Figueira J, Loureiro J, Marques J, Bianchi C, Duarte P, Ruoho M, Tittonen I and Ferreira I 2017 *ACS Appl. Mater. Interfaces* **9** 6520–9
[9] Koskinen T, Juntunen T and Tittonen I 2020 *Sensors* **20** 5188
[10] Agar J C, Lin K J, Zhang R, Durden J, Moon K S and Wong C P **2010** *Proc.—Electron. Components Technol. Conf.* pp 1226–30
[11] Wu L, Qian J, Peng J, Wang K, Liu Z, Ma T, Zhou Y, Wang G and Ye S 2019 *J. Mater. Sci. Mater. Electron.* **30** 9593–601
[12] Shih W P, Tsao L C, Lee C W, Cheng M Y, Chang C, Yang Y J and Fan K C 2010 *Sensors* **10** 3597–610
[13] Lin Q I U, Yanbo D U, Yangyang B A I, Yanhui F, Xinxin Z, Jin W U, Xiaotian W and Caihong X U 2021 *J. Therm. Sci.* **30** 465
[14] Niu X, Peng S, Liu L, Wen W and Sheng P 2007 *Adv. Mater.* **19** 2682–6
[15] Ammar S, Ramesh K, Vengadaesvaran B, Ramesh S and Arof A K 2016 *Prog. Org. Coatings* **92** 54–65
[16] Gomathi Sankar G, Sathya S, Sriyutha Murthy P, Das A, Pandiyan R, Venugopalan V P and Doble M 2015 *Int. Biodeterior. Biodegrad.* **104** 307–14
[17] Babu I and de With G 2014 *Compos. Sci. Technol.* **91** 91–97
[18] Wang Y, Zhu W, Deng Y, Fu B, Zhu P and Yu Y 2020 *Nano Energy* **73** 104773
[19] Niu D, Jiang W, Liu H, Zhao T, Lei B, Li Y, Yin L, Shi Y, Chen B and Lu B 2016 *Sci. Rep.* **6** 1–10
[20] Du Y, Li H, Jia X, Dou Y, Xu J and Eklund P 2018 *Energies* **11** 2849
[21] Brus V V, Gluba M, Rappich J, Lang F, Maryanchuk P D and Nickel N H 2018 *ACS Appl. Mater. Interfaces* **10** 4737–42
[22] Tran V and Volz S 2018 *Nanoscale* **10** 3784–91
[23] Nag A, Afasrimanesh N, Feng S and Mukhopadhyay S C 2018 *Sens. Actuators* A **271** 257–69
[24] Wei Z, Li Z, Luo P, Zhang J and Luo J 2020 *J. Alloys Compd.* **830** 154625
[25] Wang L, Jia X, Wang D, Zhu G and Li J 2013 *Synth. Met.* **181** 79
[26] Xu Y, Wang X and Hao Q 2021 *Compos. Commun.* **24** 100617
[27] Guan X and Ouyang J 2021 *CCS Chem.* **3** 2415
[28] Tao Z, Wang H, Li X, Liu Z and Guo Q 2017 *J. Appl. Polym. Sci.* **134** 1
[29] Correia A R 2019 Tailoring carbon-based materials for thermoelectric application *MSc Thesis* Universidade do Porto